

Article

Dynamic Analysis of a Delta Parallel Robot with Flexible Links and Joint Clearances

Nadia Cretescu ¹, Mircea Neagoe ^{1,*}  and Radu Saulescu ² 

¹ Renewable Energy Systems and Recycling R&D Centre, Faculty of Product Design and Environment, Transilvania University of Brasov, 500036 Brasov, Romania; ncretescu@unitbv.ro

² Design of Mechanical Elements and Systems R&D Centre, Faculty of Product Design and Environment, Transilvania University of Brasov, 500036 Brasov, Romania; rsaulescu@unitbv.ro

* Correspondence: mneagoe@unitbv.ro; Tel.: +40-268-413-000

Abstract: Delta robot is a lightweight parallel manipulator capable of accurately moving heavy loads at high speed and acceleration along a spatial trajectory. This intensive dynamic process may have a significant impact on the end-effector trajectory precision and motor behavior. The paper highlights the influence on the dynamic behavior of a Delta robot by considering individual and combined effects of clearances and friction in the spherical joints, as well as the flexibility of the rod elements. The CAD modeling of the Delta robot and its motion simulation on a representative spatial trajectory where the maximum allowed values of speed and acceleration are reached were performed using the Catia and Adams software packages. The obtained results show that the methods used were successfully applied and the effects are mutually interconnected, but not cumulative.

Keywords: parallel robot; Delta manipulator; dynamic; flexible link; joint clearance; joint friction; modelling; simulation

1. Introduction



Citation: Cretescu, N.; Neagoe, M.; Saulescu, R. Dynamic Analysis of a Delta Parallel Robot with Flexible Links and Joint Clearances. *Appl. Sci.* **2023**, *13*, 6693. <https://doi.org/10.3390/app13116693>

Academic Editor: Yutaka Ishibashi

Received: 26 April 2023

Revised: 25 May 2023

Accepted: 25 May 2023

Published: 31 May 2023



Copyright: © 2023 by the authors. Licensee MDPI, Basel, Switzerland. This article is an open access article distributed under the terms and conditions of the Creative Commons Attribution (CC BY) license (<https://creativecommons.org/licenses/by/4.0/>).

The Delta parallel robot (DPR) is a three-degree-of-freedom (3-DOF) translational manipulator that consists of a fixed base linked to a mobile platform by three arms. The first model of the Delta parallel robot was invented in 1987 by Reymond Clavel [1] as a suitable structure for high-speed and high-acceleration tasks, specially used for pick and place operations, but also for packaging, sorting, precision positioning, and other applications.

In the industry, parallel robots have light structures and usually operate at high speeds and accelerations with heavy payload; as a result, negative kinematic and dynamic effects may intervene in the operation due to joint clearances and frictions or link flexibility. Preliminary knowledge of the behavior of these robots represents a critical asset for their optimal design.

Various studies related to the analytical modeling (both kinematic and dynamic approaches) of parallel robots but also their CAD modelling and simulation can be found in the literature. To the best of our knowledge, no relevant works have been identified that address the idea of analyzing the cumulative effect of the flexibility of elastic elements in combination with the clearances and friction from the spherical joints. These three parameters can have a major role in the dynamic behavior of parallel robots. The analysis of the effects of these factors is exemplified in the paper on the case study of a Delta parallel robot (DPR).

A new DPR is proposed and developed in [2], along with its dynamic optimization. A direct and inverse pose modeling method for a DPR is addressed in [3] based on ADAMS, and a DPR kinematic model is presented in [4], completed by a closed-form inverse dynamic model using the Newton laws, a formulation called “in two spaces”. An analytical approach for the dimensional synthesis of a Delta parallel robot is presented in [5]. The analytical solution presented, with dimensional optimization for the link length, aims to find the

DPR workspace. A dynamic dimensional synthesis using the pressure/transmission angle constraints of a DPR is described in [6]. Two types of pressure angle are defined, and thus direct and indirect singularities can be identified.

The kinematic calibration and sensitivity analysis for a DPR is described in [7], a method which can be used successfully for other parallel robots.

An experimental verification of a newly developed DPR, based on the dynamic model derived by using the Hamilton's principle, is presented in [8]. An inverse dynamic model is developed using the Euler–Lagrange approach, a model validated with real torques data obtained from of a model of the Delta parallel robot developed by SIPRO [9].

Other approaches to dynamic DPR modeling are presented in [10], for example, the Lagrange equations, Newton–Euler formulation and the Principle of Virtual Work. An analysis of an analytical dynamic model of the Delta robot was presented in [11] and another analytical model was validated by experimental data [12]. Different methods for dynamic modeling of parallel robots are presented in [13–17], with numerical simulation and experimental validation.

In addition, the kinematic modeling of parallel robots, especially the Delta robot, has been extensively addressed in the literature [18–22] including forward and inverse modeling and kinematic optimization.

The numerical simulation of parallel robots is an attractive topic, mainly using MATLAB software (<https://en.wikipedia.org/wiki/MATLAB>) [23,24] or MATLAB simulation validated by experimental research [25,26].

In dynamic studies, various assumptions can be considered, such as rigid vs. flexible links (analytical or numerical), ideal condition vs. friction and clearance in joints. The effect of link flexibility is analyzed for different parallel robots by using ADAMS software (<https://hexagon.com/products/product-groups/computer-aided-engineering-software/adams>) compared with rigid link case [27–29]. An alternative approach to obtaining the analytical model of a DPR with flexible links is presented in [30].

An optimal trajectory planning for a DPR is carried out in [31] aiming to suppress robot vibration by developing an elasto-dynamic model assuming flexible links, and a polynomial function in the operating space was considered. The dynamical model of a parallel robot considering link flexibility was developed in [32] based on co-rotational and rigid finite elements.

Several scholars have analyzed the phenomenon of friction in spherical joints. The stability analysis of a ball joint based on Coulomb and Stribeck-type model was addressed in [33]. Nonlinear periodic solutions were obtained depending on the ball joint friction parameters. The error modeling for a DPR has been analyzed in [34] by considering joint clearances.

Thus, there are works that separately deal with the influence of these factors on the kinematic and dynamic behavior of the DPR, some through analytical modeling and most through numerical simulation using specialized software, but without identifying relevant results regarding the cumulative effect of these three factors (link flexibility, friction and joint clearance).

The main problems of DPR highlighted in the literature are systematized in the Introduction:

- (a) kinematic and dynamic modeling and simulation of DPR;
- (b) optimizations of the dynamic model;
- (c) new methods for solving the dynamic model;
- (d) analytical modeling with experimental verification;
- (e) the influence of the flexibility of DPR elements using different software;
- (f) the analysis of the friction in joints of DPR;
- (g) errors produced by joint clearances of DPR.

This paper addresses the following gap identified in the literature: to the best of the authors' knowledge, there is a lack of significant scientific works dealing with the cumulative effects of link flexibility, joint friction and joint clearance on the dynamic

behavior of parallel robots. Therefore, the proposed research is conducted on a Delta parallel robot using a CAD model obtained in the CATIA software (<https://en.wikipedia.org/wiki/CATIA>) and deriving specific simulations in the ADAMS software.

The rest of the paper is organized as follows: Section 2 presents the problem formulation; Section 3 proposes seven simulation scenarios and discusses the obtained results; and Section 4 draws final conclusions.

2. Problem Formulation

The effect of element flexibilities, frictions and clearances can be studied numerically by developing a CAD model of the analyzed robot in the first stage, for example, using the CATIA software, followed in the second stage by the ADAMS analysis. Since ADAMS does not easily allow the creation of elements with complex shapes, it was decided to develop the CAD model in CATIA and then export the 3D bodies (in an IGES format) to ADAMS. Thus, a CAD model can be obtained in ADAMS that reflects the properties of the existing physical robot as accurately as possible.

In this analysis, we consider the case study of a Delta Siax D3-1600 parallel robot (Figure 1a, [35]). Its simplified CAD model (without motors) at a 1:1 scale was represented in CATIA (Figure 1b) and then transferred to ADAMS (Figure 1c). The Delta Siax D3-1600 is a three degree-of-freedom (3-DOF) robot (the end-effector performs three independent translations). It is composed of a fixed platform (0) and a mobile platform (4), interconnected by three arms, A, B and C, each of them with a driving element (1) connected to the base by a motor drive (R). Each arm has a parallelogram-type kinematic chain with two flexible elements (2 and 3) and four passive spherical couples each (S_{2k1} , S_{2k2} and S_{3k1} , S_{3k2} , where $k = A, B, C$ —Figure 1d). The three arms are equiangularly distributed (Figure 1e) in relation to the global coordinate system ($X_0Y_0Z_0$) of the robot, with the origin located at point O (Figure 1d). The Delta robot has attached to the end-effector (4) a payload in the form of a cylinder (5) with a mass of 5 kg. The characteristic point P is the origin of the mobile coordinate system of the end-effector and it travels a spatial trajectory established so as to reach the maximum velocity and acceleration according to the values specified in Table 1.

Table 1. Delta SIAX D3-1600 parallel robot: main characteristics.

Parameter	Value
Total mass	80 kg
Maximum payload	5 kg
Maximum end-effector speed	8 m/s
Maximum end-effector acceleration	120 m/s ²

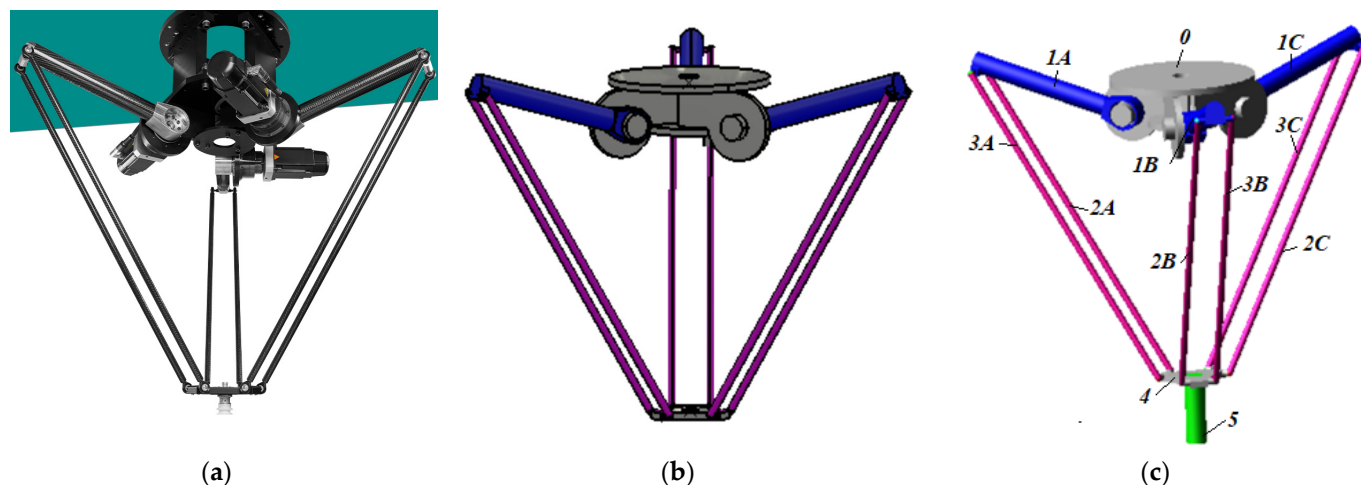


Figure 1. Cont.

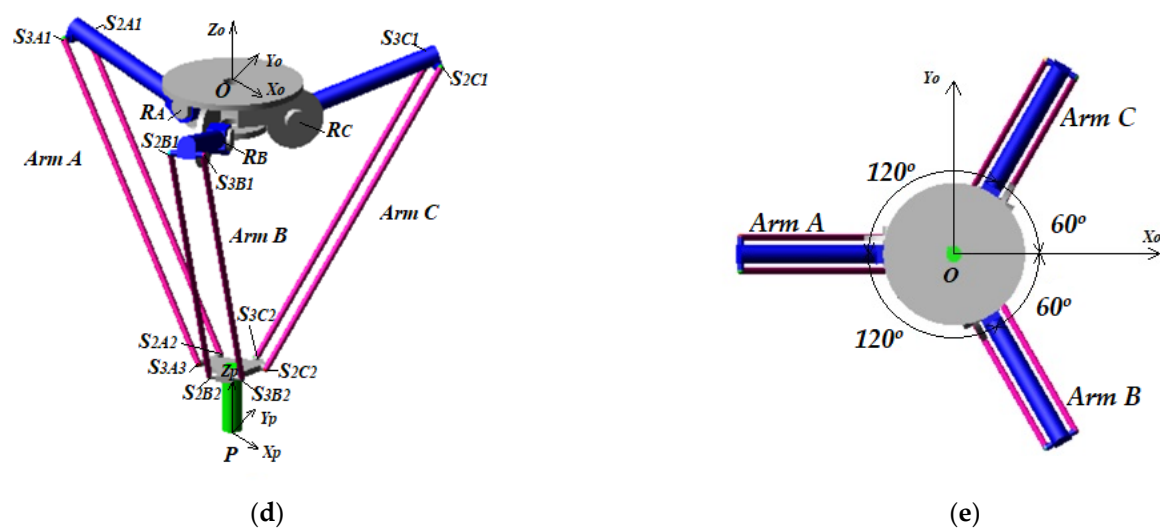


Figure 1. Delta parallel robot: (a) Delta Siax D3-1600 type robot; (b) CATIA model without payload; (c) ADAMS model with payload; (d) ADAMS model parametrisation; (e) arm arrangement.

The geometrical, mass and material properties of the robot's component bodies are key factors in determining its dynamic behavior. In the proposed analysis, the following assumptions have been made:

- Elements 0, 1, 4 and 5 are rigid solid bodies;
 - Rod Elements 2 and 3 have higher elastic characteristics than the other elements due to their dimensions, see Table 2;
 - All bodies are made of steel.

Table 2. Geometrical and mass details of the Delta robot bodies.

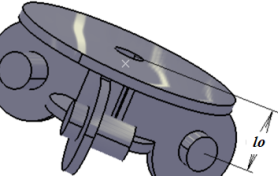
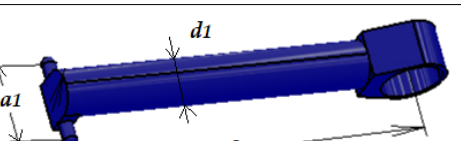
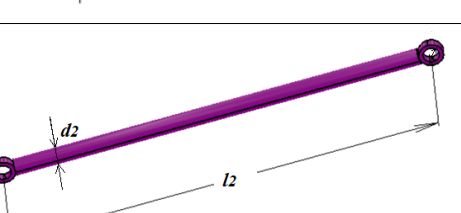
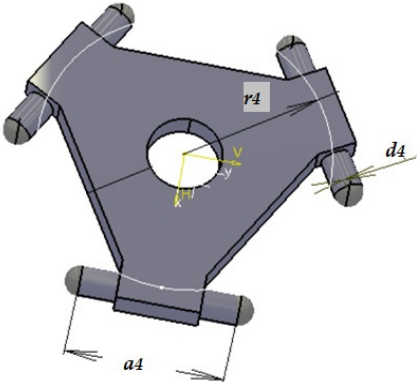
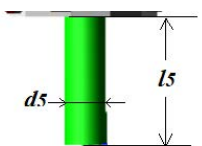
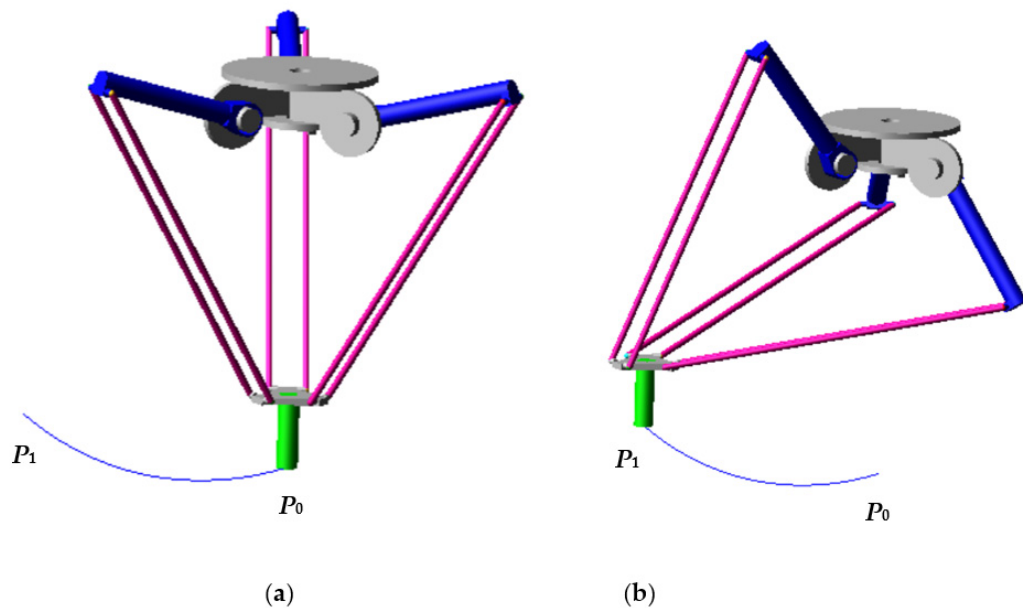
Body	CAD Model	Parameters
Fixed platform (0)		$l_0 = 125 \text{ mm}$
Crank (1)		$l_1 = 500 \text{ mm}$ $m_1 = 1.58 \text{ kg}$ $d_1 = 62 \text{ mm}$ $a_1 = 106 \text{ mm}$
Rod element (2 and 3)		$l_2 = l_3 = 1106 \text{ mm}$ $m_2 = m_3 = 0.34 \text{ kg}$ $d_2 = d_3 = 20 \text{ mm}$

Table 2. Cont.

Body	CAD Model	Parameters
Mobile platform (4)		$m_4 = 0.46 \text{ kg}$ $d_4 = 20 \text{ mm}$ $a_4 = 106 \text{ mm}$ $r_4 = 97 \text{ mm}$
Payload (5)		$l_5 = 212 \text{ mm}$ $m_5 = 5 \text{ kg}$ $d_5 = 50 \text{ mm}$

The reference model of the Delta robot is based on the assumptions of an ideal mechanism, where all bodies are rigid solids, all kinematic joints are ideal (no clearance, no friction), and the characteristic point P follows a trajectory that reaches maximum allowed values of speed and acceleration. Thus, the fifth degree polynomial function was chosen to generate the movement trajectory in the joint space as well as a short trajectory travel time of 0.2 s, the time resulting from the simultaneous provision of the conditions for the robot to touch the P_0P_1 trajectory (Figure 2), the maximum speed of the end-effector $v_{Pmax} = 8 \text{ m/s}$ and the maximum acceleration $a_{Pmax} = 120 \text{ m/s}^2$ (see Table 1).

**Figure 2.** Cartesian trajectory of the Delta robot: (a) initial position; (b) final position.

The starting position of the Cartesian trajectory (P_0) corresponds to the initial position of the robot where all three motor torques R_A , R_B and R_C are in the zero position and Elements 1 are arranged in a horizontal plane (parallel to X_0Y_0 , see Figure 1d). The trajectory in the Cartesian space P_0P_1 is a spatial curve obtained by applying an angular

displacement of 70° in the positive direction of the joint axis R_A , 41° in the positive direction of the coupling axis R_B and of 36° in the negative direction of the joint axis R_C (Figure 3a). Along this trajectory, the maximum angular velocity of $656^\circ/\text{s}$ in joint A, $384^\circ/\text{s}$ in joint B and $292^\circ/\text{s}$ in joint C is reached (Figure 3b), as well as the maximum angular accelerations of $10,103^\circ/\text{s}^2$ (engine A), $5124^\circ/\text{s}^2$ (engine B) and $4500^\circ/\text{s}^2$ (engine C), as shown in Figure 3c.

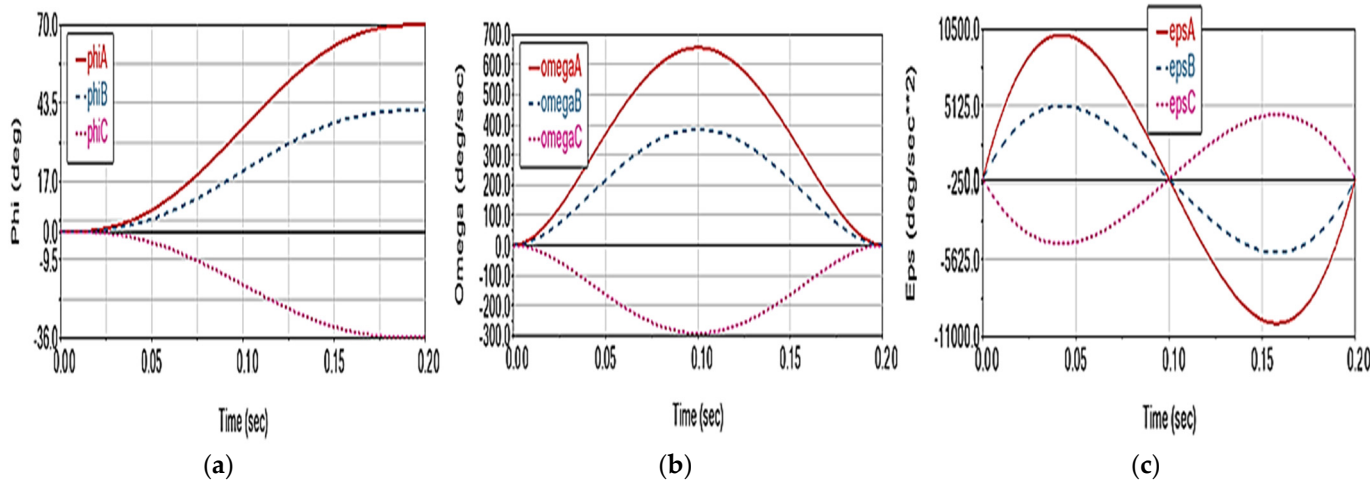


Figure 3. Motion trajectories in the active joint space (R_A , R_B and R_C): (a) angular displacement; (b) angular velocity and (c) angular acceleration.

When polynomial movement trajectories of the fifth degree are applied to the active joints, a Cartesian trajectory P_0P_1 is obtained. This trajectory is characterized by the displacement of the characteristic point P along all three axes of the global coordinate system $X_0Y_0Z_0$ (Figure 4), and it reaches a final position of $r_P = 1.245 \text{ m}$ (Figure 5a). The trajectory also reaches a maximum speed of $v_P = 8 \text{ m/s}$ at 0.1 s (Figure 5b) and a maximum acceleration of $a_P = 120 \text{ m/s}^2$ at approximately 0.052 s and 0.158 s (Figure 5c).

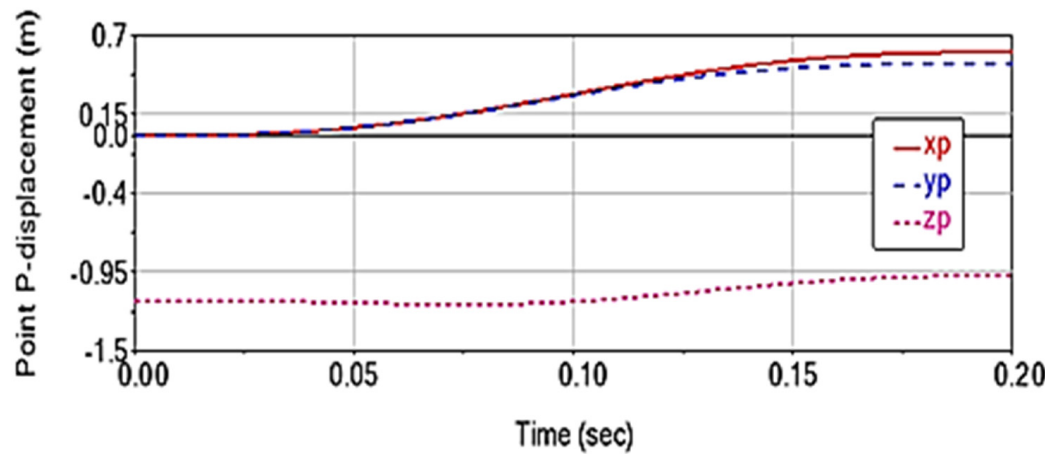


Figure 4. End-effector displacement components for the Delta robot reference model.

The torque in the active joints (Figure 6) on the stated trajectory has the allure of angular acceleration (see Figure 3c); higher values of the moment TA are observed due to the higher angular accelerations (and consequently higher values of angular speeds and displacements) compared to the other two active torques.

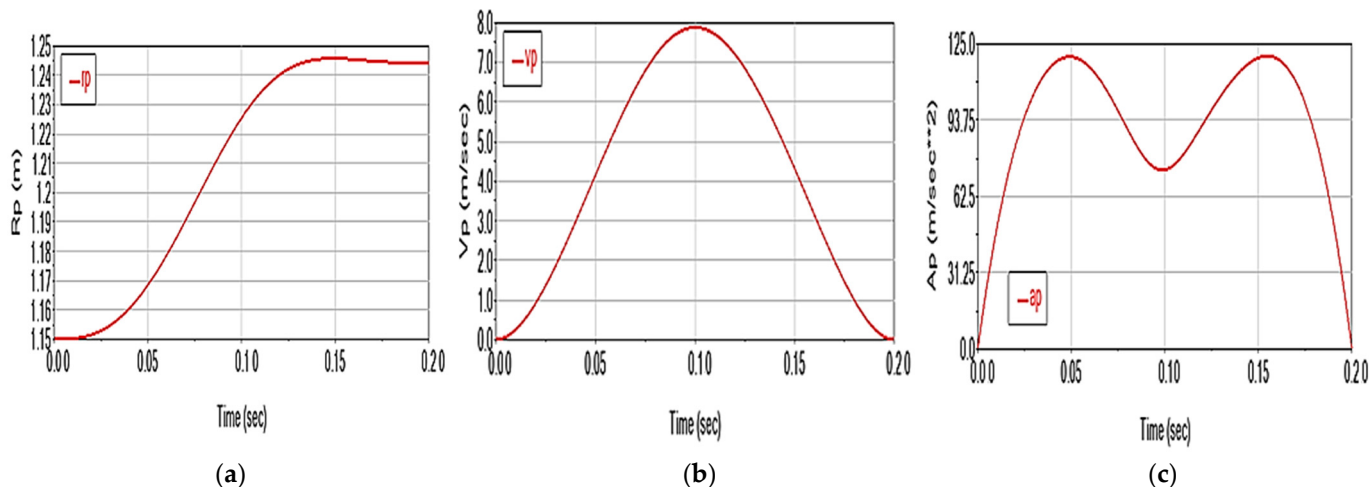


Figure 5. End-effector motion for the Delta robot reference model (magnitude of): (a) displacement; (b) velocity and (c) acceleration.

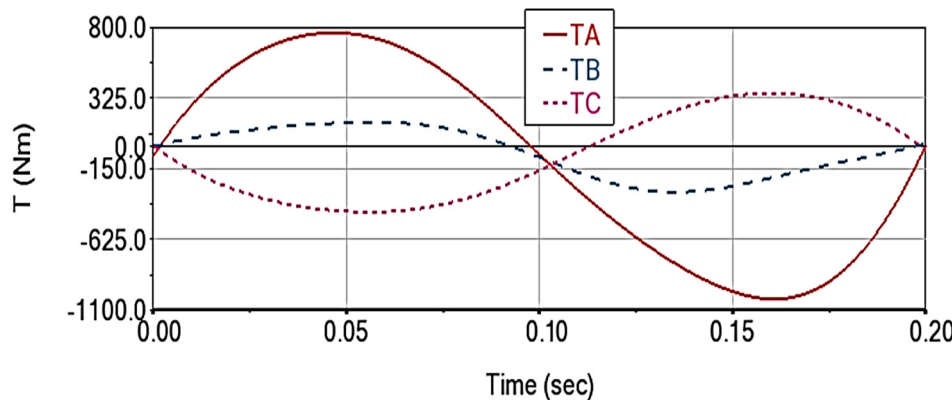


Figure 6. Driving torques (T_A , T_B and T_C) for the Delta robot reference model.

Under these considerations, the aim of this study is to analyze the kinematic and dynamic effects of these three factors, both individually and in combination:

- Friction on spherical joints;
- Clearances on spherical joints;
- Elasticity of the flexible rod elements (2 and 3).

Thus, the comparative analysis of the Delta robotic structure is presented in seven dynamic simulation scenarios, taking as reference the previously defined ideal model. The study makes the following assumptions:

- Scenario 1: considers only the frictions from the passive spherical joints (S_2k_1 , S_2k_2 and S_3k_1 , S_3k_2 , $k = A, B, C$) assuming steel/steel friction with lubricant.
- Scenario 2: considers only the elasticity of Elements 2 and 3 and only allows natural frequencies lower than 250 Hz.
- Scenario 3: considers only the play in the passive spherical joints with the value of 0.1 mm.
- Scenario 4: combines Scenario 1 and Scenario 2.
- Scenario 5: combines Scenario 1 and Scenario 3.
- Scenario 6: combines Scenario 2 and Scenario 3.
- Scenario 7: combines Scenario 1, Scenario 2 and Scenario 3.

3. Results and Discussions

The influence of each of the three factors considered (Scenarios 1–3) as well as their combination (Scenarios 4–7) was analyzed by comparison with the reference model (ideal case) in order to identify

- (a) kinematic (displacements, speeds and accelerations of the characteristic point) and dynamic (driving torques) deviations generated by these factors. These deviations are denoted generically with $e_X_p = X_p - X$, where $X = r_p, v_p, a_p, TA, TB, TC, p$ is the considered parameter (μ —friction, e —elasticity, c —clearance), and X_p is the value of the X variable in the assumption of considering the p factor, X obtained in the ideal case;
- (b) the coupling effect of the factors, i.e., the extent to which they are independent variables and whether their effects can be considered additive phenomena.

3.1. Scenario 1

In this scenario, we start from the ideal case of the robot structure, to which the friction in the spherical joints S_{2k1}, S_{2k2} and $S_{3k1}, S_{3k2}, k = A, B, C$ is added, taking into account steel/steel friction with lard oil lubricant with the 0.11 static friction coefficient and the 0.084 dynamic coefficient [36].

As is known, friction in kinematic joints does not influence the motion transmission function but has an effect on the dynamic behavior of the robot. The friction from the spherical joints has a moderate effect on the driving torques (about 0.007%, Figure 7), resulting in deviations of up to 0.508 N·m for TA (Figure 7a), 0.207 N·m for TB (Figure 7b) and 0.241 N·m for TC (Figure 7c).

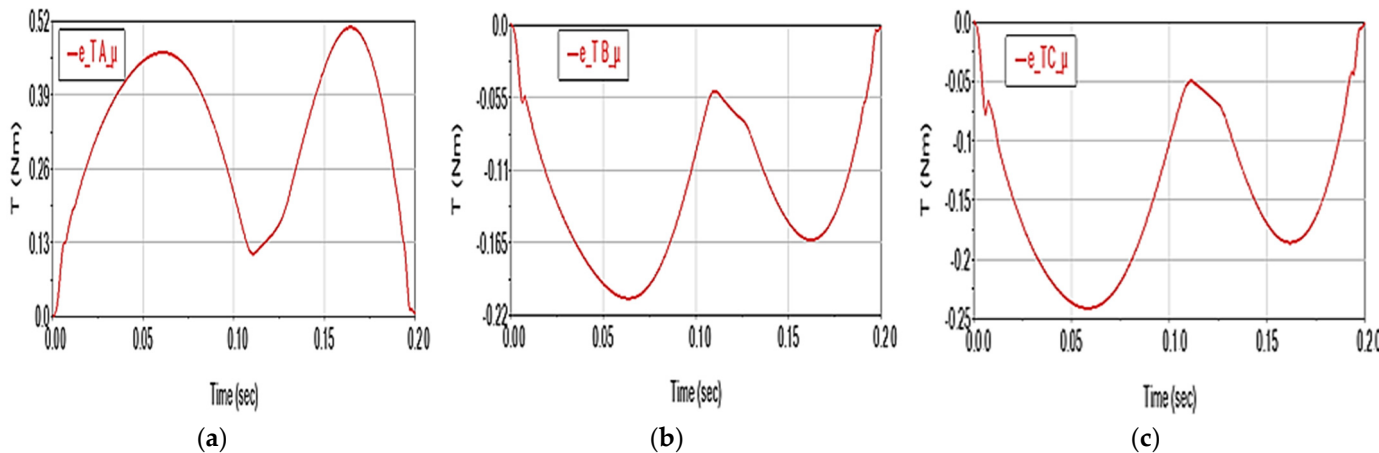


Figure 7. The driving torque deviations in the hypothesis of considering the friction from the spherical joints (Scenario 1): (a) arm A; (b) arm B; (c) arm C.

A variation of these deviations is noted for all three driving torques, with a profile similar to the acceleration a_p (see Figure 5c) and in correlation with the moment variation (Figure 6):

- the deviation values $e_Tk\mu, k = A, B, C$ are directly proportional to the absolute values of the moments Tk ;
- friction leads to an increase in the driving torques value during the acceleration phase (0.0–0.1 s interval) and helps the motors to brake during the deceleration phase (0.1–0.2 s).

3.2. Scenario 2

In the hypothesis of considering the flexibility of the flexible elements of the Delta parallel robot (Elements 2 and 3 on each arm, see Figure 8) and limiting the analysis to the first 10 vibration modes (with natural frequencies lower than 250 Hz, as the effect of

higher frequencies is negligible—the principal characteristics are presented in Figure 9), the results represented in Figure 10 (motion deviations) and Figure 11 (torque deviations) are obtained.

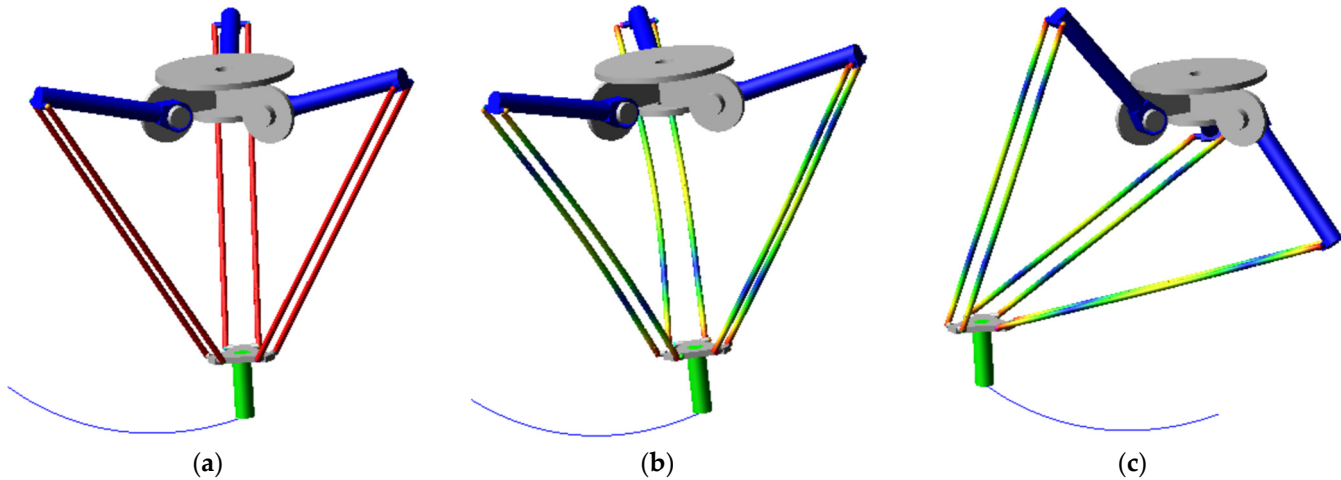


Figure 8. The CAD model of the Delta robot: (a) in ideal case, and with flexible links at (b) trajectory start point P_0 ; (c) trajectory end point P_1 .

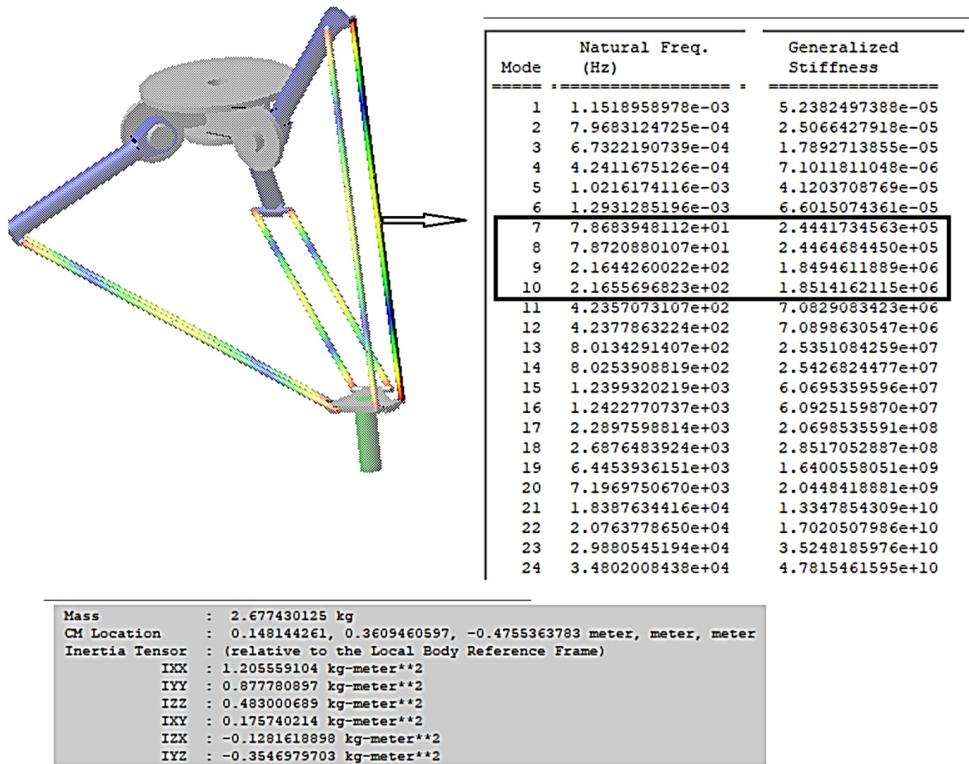


Figure 9. The principal modes of vibration (Hz), generalized stiffness (N/m) and mass properties (including CM and inertia tensor) of rods.

Taking into account the natural properties of the rod elements (Table 2), the ADAMS dynamic simulation leads to low deviations from the theoretical trajectory of the effector ($e_{rp} < 4.2 \cdot 10^{-6}$ m, Figure 10a), the speed deviation of up to $3.1 \cdot 10^{-4}$ m/s for (Figure 10b) and deviations of up to 5 m/s² for acceleration (i.e., max. 4.2%, Figure 10c). The largest deviations e_{vp} and e_{ap} occur at around 0.042 s and 0.158 s, respectively, the moments of time at which the acceleration a_p is at its maximum (see Figure 5c).

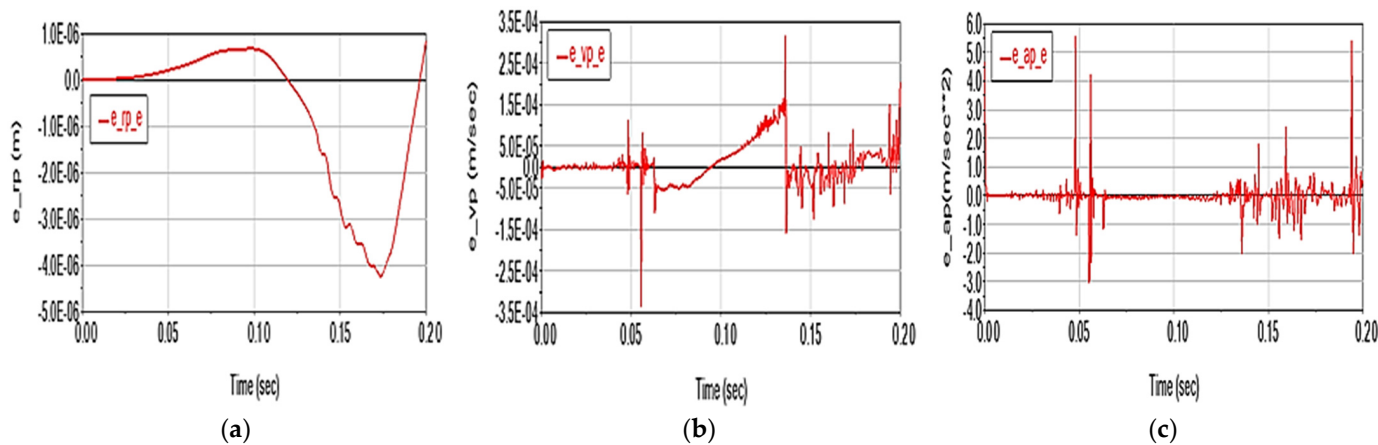


Figure 10. Kinematic deviations in Scenario 2 for (a) displacement; (b) velocity and (c) acceleration.

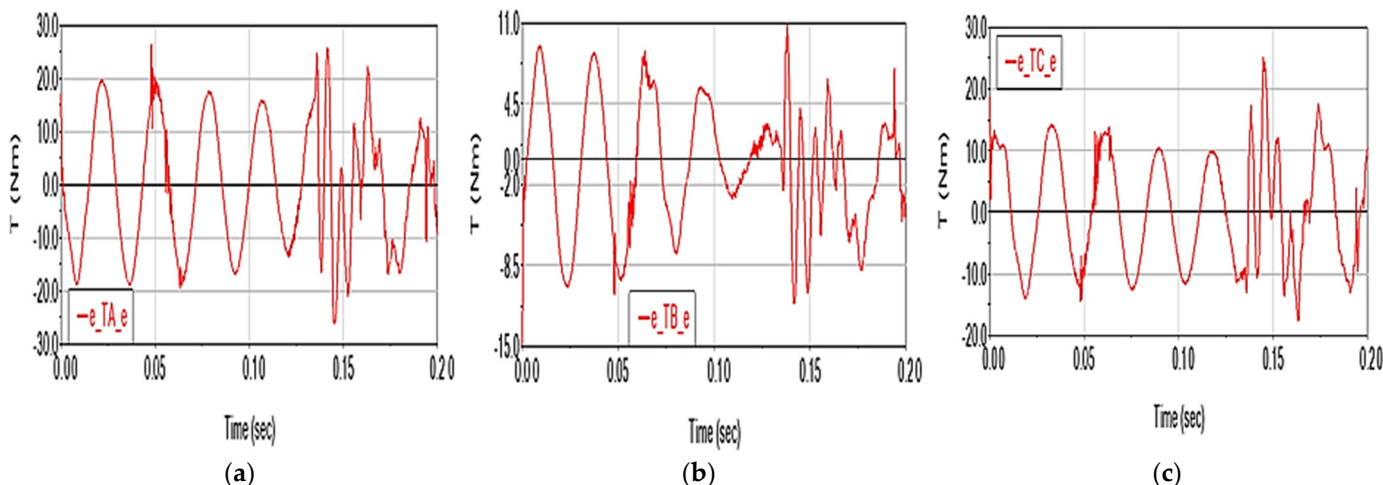


Figure 11. Driving torque deviations in Scenario 2 for (a) arm A; (b) arm B and (c) arm C.

The driving torque deviations have an oscillatory evolution (seven oscillations with a period of approx. 0.025 s) characterized by maximum values of ~ 26.4 N·m for TA (Figure 11a), ~ 10.8 N·m for TB (Figure 11b) and ~ 25.3 N·m for TC (Figure 11c). The maximum deviations are recorded in the case of the engine in joint A ($\sim 0.035\%$). An instability phenomenon occurs at the time of ~ 0.15 s, corresponding to the maximum acceleration zone of the characteristic point.

3.3. Scenario 3

In this subsection, we analyze the influence of the clearances in the spherical, using a single value of 0.1 mm for all 12 joints S_{2k1}, S_{2k2} and S_{3k1}, S_{3k2} , $k = A, B, C$. Under these conditions, the deviation of the characteristic point in the initial position is 0.2 mm.

The deviation from the characteristic point trajectory is up to $1.18 \cdot 10^{-4}$ m (Figure 12a), with a velocity deviation of up to 0.0035 m/s (Figure 12b) and an acceleration of up to 0.068 m/s² (Figure 12c). Compared to Scenario 2, the displacement deviation on the trajectory is significantly higher (~ 20 times higher), but the deviation of the acceleration on the trajectory is much lower (~ 70 times lower).

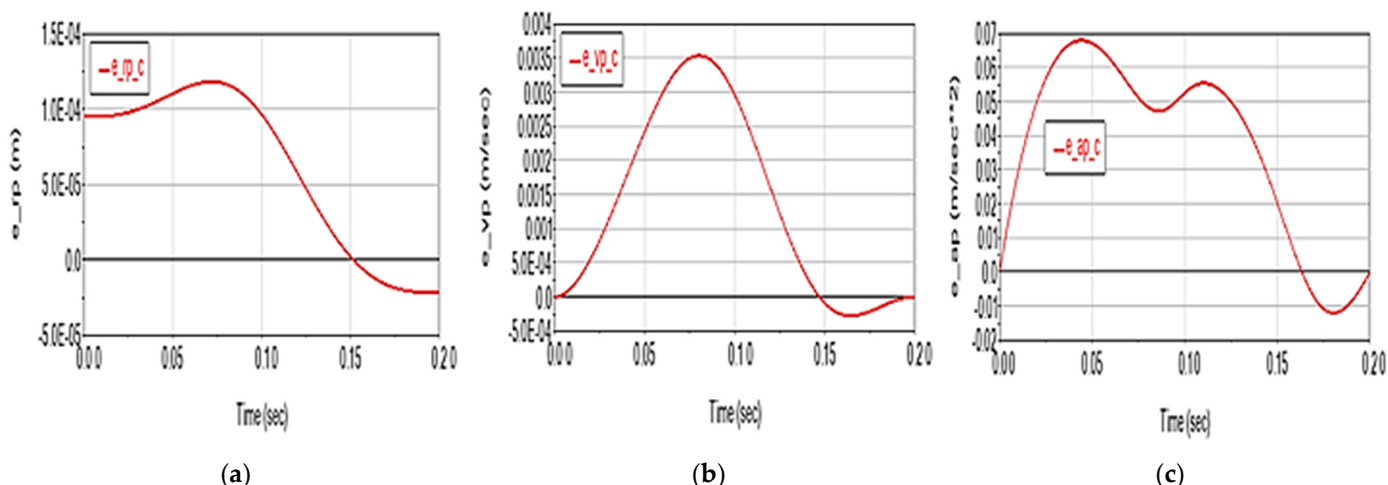


Figure 12. Kinematical deviation in Scenario 3 for (a) displacement; (b) velocity and (c) acceleration.

The influence of the spherical joint clearances on the driving torques is moderate, about 10–20 times lower than in Scenario 2, but 2–3 times higher than in Scenario 1. A deviation of up to 1.7 N·m can be highlighted for TA (Figure 13a), up to 0.49 N·m for TB (Figure 13b) and up to 0.47 N·m for TC (Figure 13c). The extreme values of the deviations are also recorded around the values of 0.042 s and 0.158 s, which are co-responsible for the extreme values of the driving motors (Figure 6).

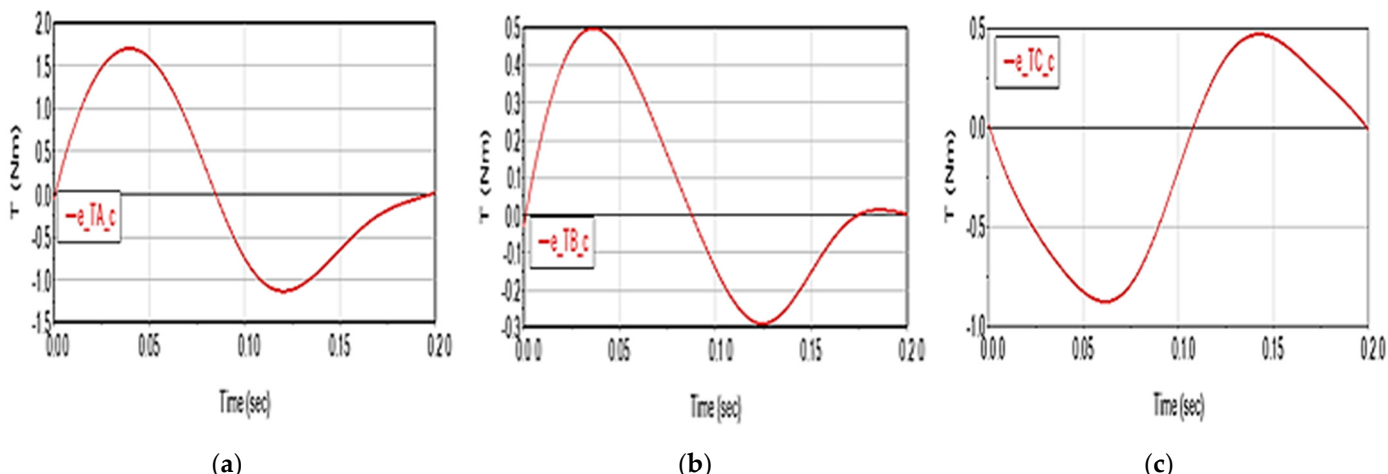


Figure 13. Driving torque deviations in Scenario 3 for (a) arm A; (b) arm B and (c) arm C.

3.4. Scenario 4

In this subsection, we analyze the cumulative influence of friction in the spherical joints and elasticity of the rod elements. We compare and analyze the cumulative resulting deviations with the sum of the deviations identified in Scenarios 1 and 2 to identify the coupling effect between these two factors.

Figure 14 shows the kinematic behavior of the Delta robot with the elastic elements and the joint friction, highlighting both the deviations of the effector motion from the ideal case (red, solid line) and the differences from the case of summing the separate effects of the two factors (blue, dashed line). For the characteristic point displacement (Figure 14a), it can be observed that the cumulative effect of the factors leads to a deviation (in absolute value) of up to a maximum of $4.23 \cdot 10^{-6}$ m (compared to a maximum of $\sim 4 \cdot 10^{-6}$ m for the case of summing the effects), up to $4.2 \cdot 10^{-4}$ m/s for velocity (Figure 14b) compared to the maximum of $3.5 \cdot 10^{-4}$ m/s for the additive case, and up to ~ 6 m/s² for acceleration (Figure 14c) compared to the maximum ~ 6 m/s² for the case of summing the effects. These

results highlight that the kinematic effects of the two factors (friction in the spherical joints and the elasticity of the elements) are not additive.

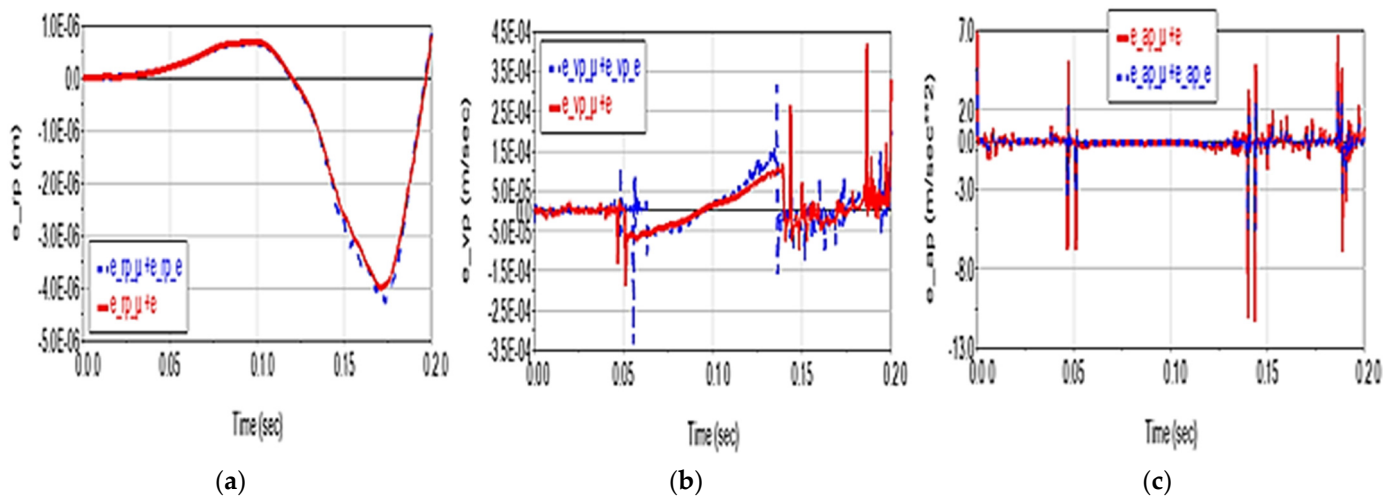


Figure 14. Motion deviations in Scenario 4 (red solid line) and the additive effect of friction and elasticity factors (blue dashed line) for (a) displacement; (b) velocity and (c) acceleration.

Similar to the motion case, the cumulative effect of the two factors results in a decrease in the maximum values of the driving torque deviations compared to the additive case (Figure 15). Therefore, it can be concluded that these factors have no significant coupling effect. Friction (with less significance) does not affect the shape of the deviation curve, but rather contributes to better curve shapes for the torque deviation values.

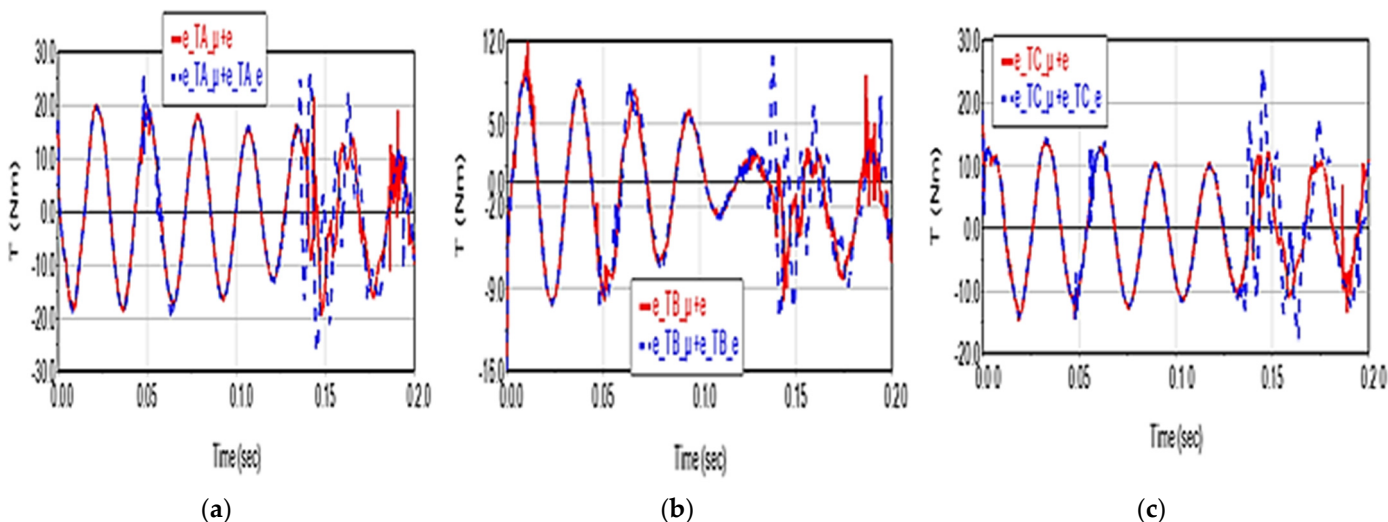


Figure 15. Driving torque deviations in Scenario 4 (red solid line) and the additive effect of friction and elasticity factors (blue dashed line) for (a) arm A; (b) arm B and (c) arm C.

3.5. Scenario 5

The kinematic deviations from the theoretical movement trajectory are shown in Figure 16. In the case of displacement, it can be seen that the cumulative effect of these two factors leads to a deviation similar to that observed in the simulative case. As a result, the effects of the two factors on the kinematic behavior of the Delta parallel robot are not cumulative and their coupling results in the same deviations.

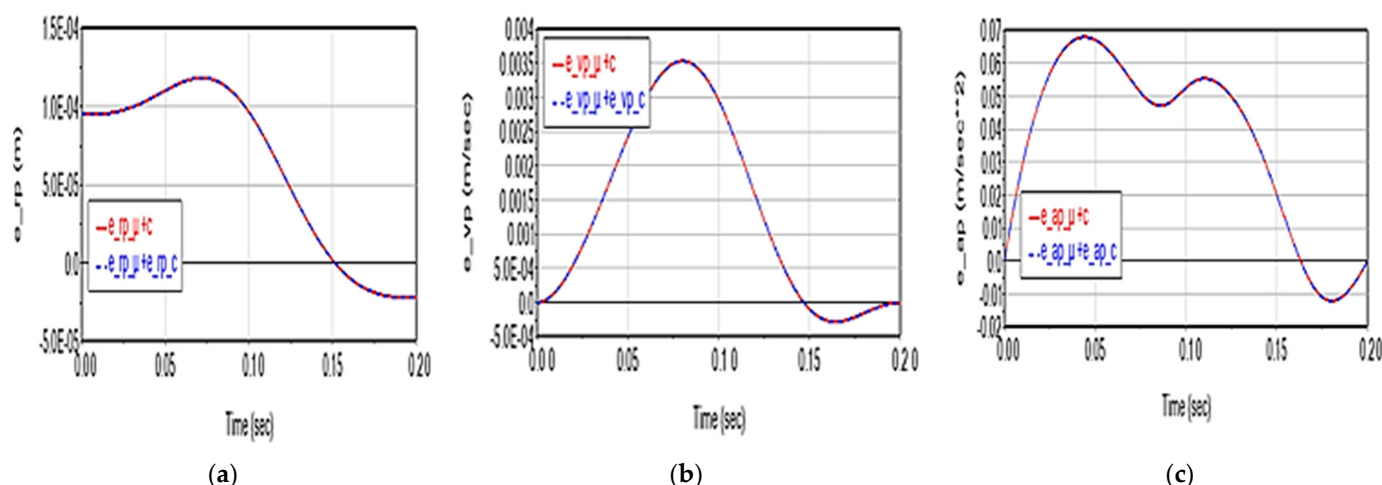


Figure 16. Motion deviations in Scenario 5 (red solid line) and the additive effect of friction and clearance factors (blue dashed line) for (a) displacement; (b) velocity and (c) acceleration.

The cumulative effect of the two factors manifests similarly in the case of motor moments: it leads to the increase in deviations up to 2.12 N·m (additive case) for TA torque (Figure 17a), up to 0.36 N·m (TB torque, Figure 17b), 1.11 N·m (TC torque, Figure 17c). The moment deviations still have the same value also in the case of summing the effects, when their values are the same compared to the case of summing the effects, without affecting the shape of the curves.

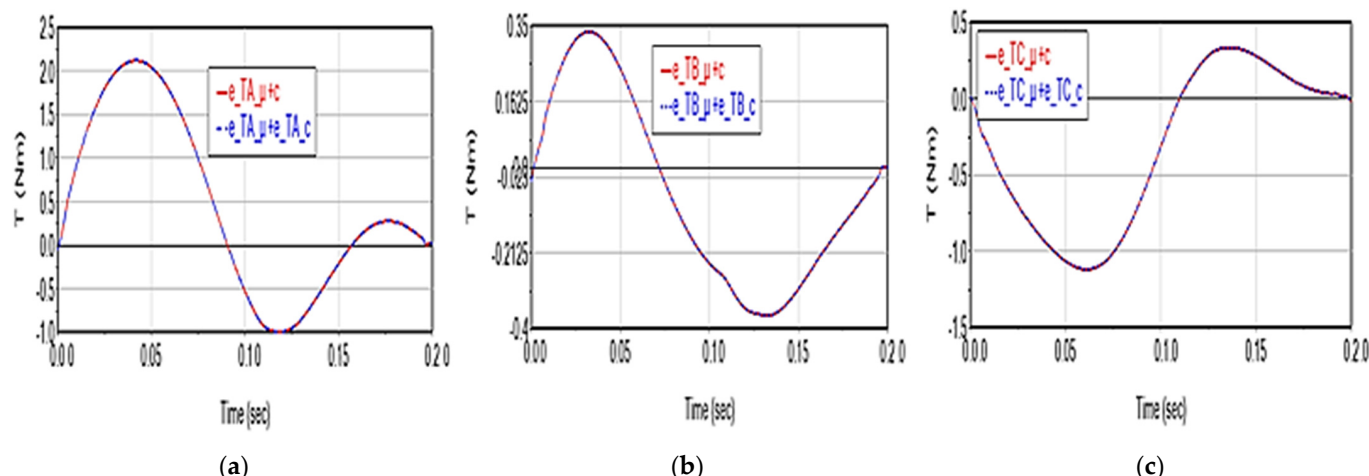


Figure 17. Driving torque deviations in Scenario 5 (red solid line) and the additive effect of friction and clearance factors (blue dashed line) for (a) arm A; (b) arm B and (c) arm C.

3.6. Scenario 6

The combination between the flexibility of the rod elements and the clearances in the spherical joints (0.1 mm) has almost no effect in the displacement and velocity of the characteristic point. However, the “picks” in the acceleration are considered reduced and the cumulative effect is taken into consideration (Figure 18).

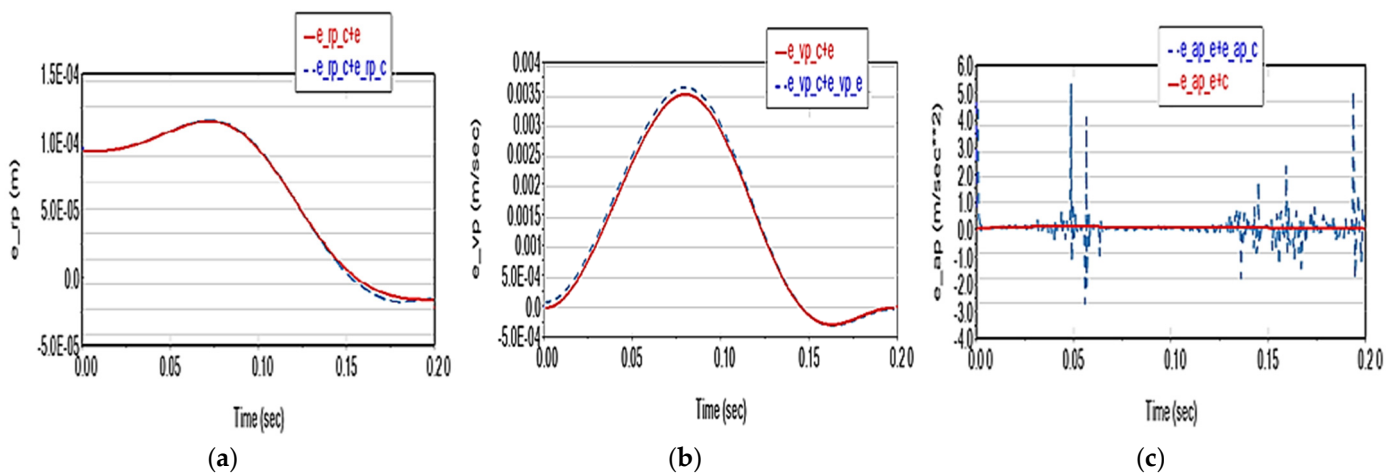


Figure 18. Motion deviations in Scenario 6 (red solid line) and the additive effect of clearance and elasticity factors (blue dashed line) for (a) displacement; (b) velocity and (c) acceleration.

In this scenario, the moment deviations have a relatively constant harmonic pitch and amplitude variation, the maximum values reaching ~ 50 N·m vs. ~ 20 N·m (in the additive case) for TA (Figure 19a), to ~ 30 N·m vs. ~ 10 N·m for TB (Figure 19b), 20 N·m vs. 22 N·m for TC (Figure 19c).

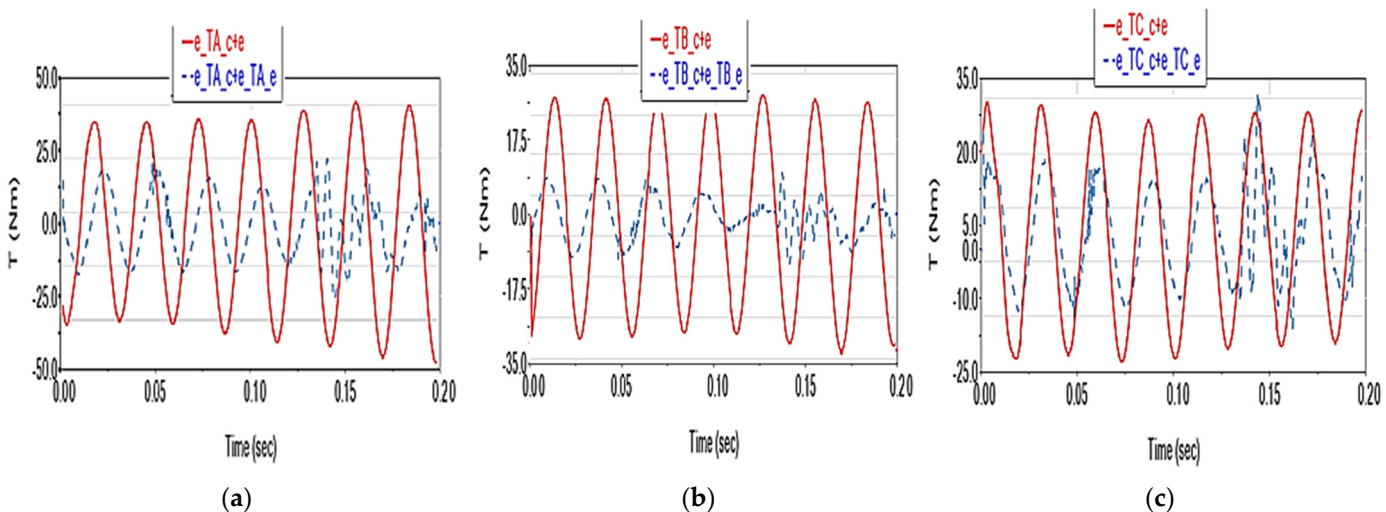


Figure 19. Driving torque deviations in Scenario 6 (red solid line) and the additive effect of clearance and elasticity factors (blue dashed line) for (a) arm A; (b) arm B and (c) arm C.

3.7. Scenario 7

In this scenario, the cumulative effects of the three factors (friction, flexibility and clearance) on the kinematic and dynamic behavior of the Delta robot are not considered. ADAMS simulations that consider the simultaneous action of those three factors resulted in values of kinematic deviations that are approximately the same values for displacement and speed (Figure 20). However, for acceleration, smaller values are emphasized due to the better numerical integration in ADAMS compared to summing the deviations generated individually by each factor (Figure 20c).

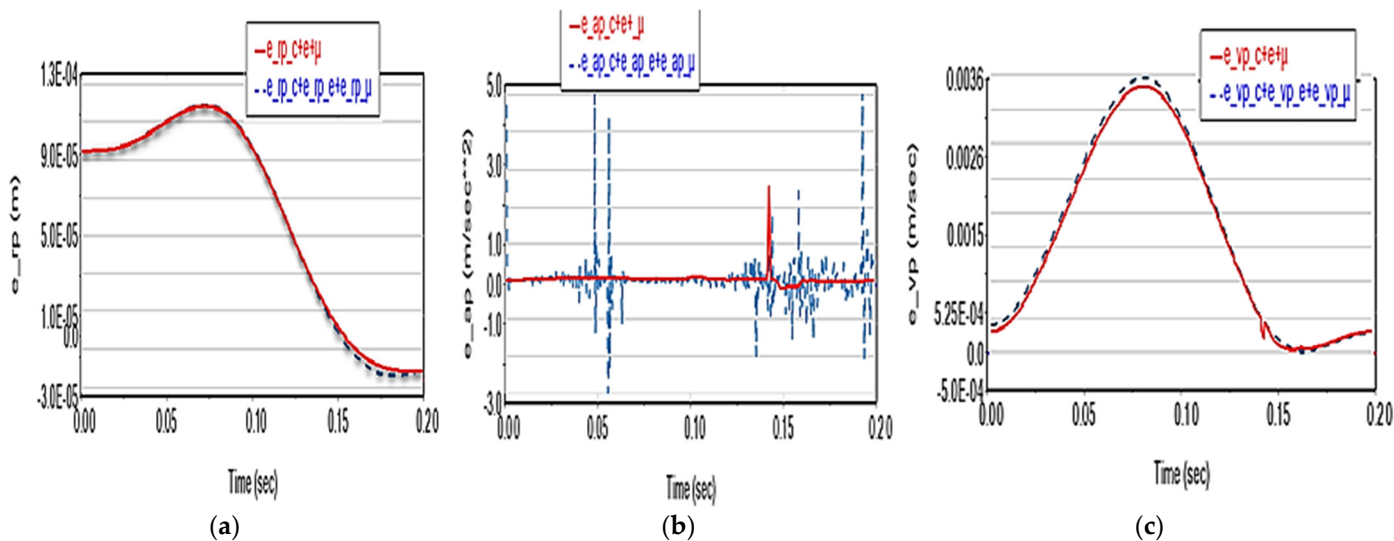


Figure 20. Motion deviations in Scenario 7 (red solid line) and the additive effect of friction, elasticity and clearance factors (blue dashed line) for (a) displacement; (b) velocity and (c) acceleration of the characteristic point.

The maximum deviation of the driving torques shows the same type of harmonic variation as in the scenarios where the elasticity factor is considered. It reaches ~ 120 N·m vs. ~ 20 N·m (in the additive case) for TA (Figure 21a), ~ 80 N·m vs. ~ 10 N·m for TB (Figure 21b) and ~ 70 N·m vs. ~ 10 N·m for TC (Figure 21c).

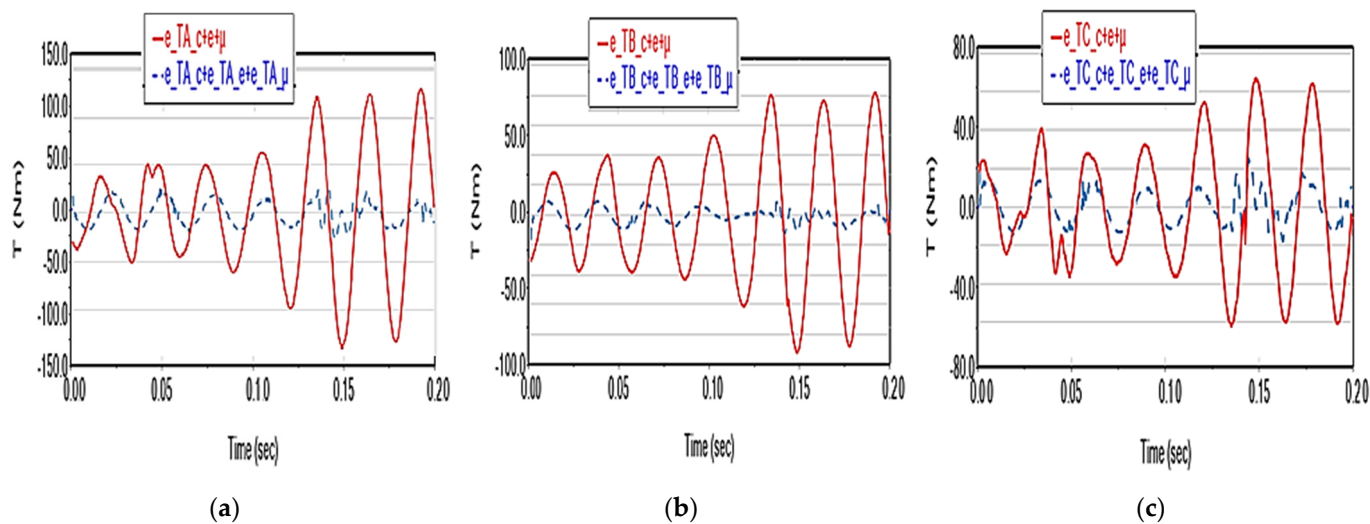


Figure 21. Driving torque deviations in Scenario 7 (red solid line) and the additive effect of clearance, friction and elasticity factors (blue dashed line) for (a) arm A; (b) arm B and (c) arm C.

4. Conclusions

A new approach is employed in this paper by analyzing the impact of three factors on the kinematic and dynamic behavior of the Delta parallel robot: the elasticity of the robot's supple elements (rod elements), friction and clearance in the spherical joints. For this purpose, the analysis was carried out for the case study of a Delta SIAX 3-1600-type robot based on the 3D models developed in CATIA and simulated in the ADAMS software.

The following summarizes the effects of these factors' actions on the movement trajectory:

- Friction has an insignificant influence on the movement parameters of the characteristic point (displacement, speed, acceleration);

- The elasticity of the elements causes practically negligible deviations in the displacement on the trajectory (of the order of 10^{-6} m), small deviations on velocity (of the order of 10^{-4} m/s), but significant in the acceleration (of up to 5 m/s^2);
- Joint clearances (considered at the value of 0.1 mm) have a substantial effect on the characteristic point displacement (deviations of the order of 10^{-4} m), moderate on velocity (of the order of 10^{-3} m/s) and relatively negligible on acceleration (of order 10^{-2} m/s^2);
- The coupling of any two of these factors results in the cumulative effects on kinematics and dynamics, except in Scenario 6, where the deviations reach values three times higher than those in the case of the individual effects summation;
- The coupling of the three factors leads, from a kinematic point of view, to a slight reduction in deviations, except for acceleration, where a significant reduction in deviations, and especially in picks, can be observed, leading to a better numerical integration solution;
- Regarding dynamics, the effects of the three factors are the following:
- Friction in the joints causes a practically insignificant variation in the driving torques (of the order of 10^{-1} N·m) compared to their nominal values of the order of 10^3 N·m (<750 N·m);
- The elasticity of the elements has a substantial impact on driving torques (deviations of up to 25 N·m, i.e., 3.3%, with a harmonic evolution);
- Joint clearances have a moderate effect on driving torques (<2 N·m);
- When two factors are combined (except in Scenario 6), the deviations can reach values up to two times higher compared to the case of the summation of individual effects and values up to three times higher when all three factors are combined.

For all factor coupling scenarios (S4–S7), the study observed that individual effects are not always cumulative. The coupling of factors can increase deviation values when the clearances and elasticities in the joints are considered simultaneously. Consequently, it is not recommended to simulate these factors separately and sum their effects. Since the phenomena are not linear, a combined approach of the factors is necessary to obtain relevant results. The authors propose to validate the conclusions of this theoretical study resulting from numerical simulations in the ADAMS software through experimental means in the future.

Author Contributions: Conceptualization, M.N. and N.C.; methodology, N.C., M.N. and R.S.; software, N.C. and R.S.; validation, M.N., N.C. and R.S.; formal analysis, M.N. and N.C.; investigation, N.C. and R.S.; resources, N.C., M.N. and R.S.; data curation, M.N. and R.S.; writing—original draft preparation, N.C.; writing—review and editing, M.N. and R.S.; visualization, N.C. and R.S.; supervision, M.N. All authors have read and agreed to the published version of the manuscript.

Funding: This research received no external funding.

Institutional Review Board Statement: Not applicable.

Informed Consent Statement: Not applicable.

Data Availability Statement: Not applicable.

Conflicts of Interest: The authors declare no conflict of interest.

References

1. Clavel, R. Dispositif Pour le Déplacement et le Positionnement d'un Élément dans L'espace. Google Patents WO1987003528A1, 18 June 1987.
2. Angel, L.; Bermudez, J.; Munoz, O. Dynamic optimization and building of a parallel delta-type robot. In Proceedings of the International Conference on Robotics and Biomimetics, Shenzhen, China, 12–14 December 2013; pp. 444–449. [CrossRef]
3. Zhang, J.; Shi, L.; Gao, R.; Lian, C. A Method for obtaining direct and inverse pose solutions to Delta parallel robot based on ADAMS. In Proceedings of the International Conference on Mechatronics and Automation, Changchun, China, 9–12 August 2009; pp. 1332–1336. [CrossRef]

4. Guglielmetti, P.; Longchamp, R. A closed form inverse dynamics model of the delta parallel robot. *IFAC Proc. Vol.* **1994**, *27*, 51–56. [[CrossRef](#)]
5. Dastjerdi, A.H.; Sheikhi, M.M.; Masouleh, M.T. A complete analytical solution for the dimensional synthesis of 3-DOF delta parallel robot for a prescribed workspace. *Mech. Mach. Theory* **2020**, *153*, 103991. [[CrossRef](#)]
6. Zhang, L.; Mei, J.; Zhao, X.; Huang, T. Dimensional synthesis of the Delta robot using transmission angle. *Robotica* **2011**, *30*, 343–349. [[CrossRef](#)]
7. Huiping, S.; Qingmei, M.; Ju, L.; Jiaming, D.; Guanglei, W. Kinematic sensitivity, parameter identification and calibration of a non-fully symmetric parallel Delta robot. *Mech. Mach. Theory* **2021**, *161*, 104311.
8. Miller, K. Experimental Verification of Modeling of Delta Robot Dynamics by Direct Application of Hamilton’s Principle. In Proceedings of the IEEE International Conference on Robotics and Automation (ICRA), Nagoya, Japan, 21–27 May 1995; pp. 532–537.
9. Falezza, F.; Vesentini, F.; Di Flumeri, A.; Leopardi, L.; Fiori, G.; Mistrorigo, G.; Muradore, R. A novel inverse dynamic model for 3-DoF delta robots. *Mechatronics* **2022**, *83*, 102752. [[CrossRef](#)]
10. Brinker, J.; Corves, B.; Wahle, M. A comparative study of inverse dynamics based on clavel’s delta robot. In Proceedings of the 14th World Congress in Mechanism and Machine Science, Taipei, China, 25–30 October 2015; pp. 25–30.
11. Codourey, A. Dynamic modelling and mass matrix evaluation of the delta parallel robot for axes decoupling control. In Proceedings of the IEEE/RSJ International Conference on Intelligent Robot and Systems, Osaka, Japan, 4–8 November 1996; Volume 3, pp. 1211–1218.
12. Asadi, F.; Heydai, A. Analytical dynamic modeling of Delta robot with experimental verification. *Proc. Inst. Mech. Eng. Part K J. Multi-Body Dyn.* **2020**, *234*, 623–663.
13. Rat, N.R.; Neagoe, M.; Gogu, G.; Stan, S.D. Dynamic analysis of an Isoglide3-T3 parallel robot. In Proceedings of the Annals of DAAAM 2009 & Proceedings of the 20th International DAAAM Symposium “Intelligent Manufacturing & Automation: Theory, Practice & Education”, Vienna, Austria, 25–28 November 2009; p. 15.
14. Cretescu, N.; Neagoe, M. Dynamic Modelling of an Isoglide T3 Type Parallel Robot. In *New Advances in Mechanisms, Mechanical Transmissions and Robotics MTM&Robotics*; Springer International Publishing: Cham, Switzerland, 2020; pp. 235–248. [[CrossRef](#)]
15. Rat, N.R.; Neagoe, M.; Stan, S.D. Comparative Dynamic Analysis of Two Parallel Robots. In *Solid State Phenomena*; Trans Tech Publications Ltd.: Stafa-Zurich, Switzerland, 2010; pp. 345–356.
16. Rat, N.; Neagoe, M.; Gogu, G. Theoretical and Experimental Research on the Dynamics of a 4DOF Isoglide 4-T3R1 Parallel Robot. In Proceedings of the SYROM 2009: 10th IFToMM International Symposium on Science of Mechanisms and Machines, Brasov, Romania, 12–15 October 2009; pp. 387–396. [[CrossRef](#)]
17. Rat, N.R.; Neagoe, M.; Diaconescu, D.; Stan, S.D. Dynamic analysis of a Triglide parallel robot. In Proceedings of the 4th International Conference on Human System Interaction (HSI), Yokohama, Japan, 19–21 May 2011; pp. 245–249.
18. Robert, L.; Williams, I.I. The Delta Parallel Robot: Kinematics Solutions, Mechanical Engineering. Ph.D. Thesis, Ohio University, Athens, Ohio, 2016.
19. Hamdoun, O.; Bakkali, L.E.; Baghli, F.Z. Analysis and Optimum Kinematic Design of a Parallel Robot. In Proceedings of the 10th International Conference Interdisciplinarity in Engineering, Tîrgu Mureş, Romania, 6–7 October 2016.
20. Hugo, H.; Joan, L. The Forward and Inverse Kinematics of a Delta Robot, Chapter. In Proceedings of the Advances in Computer Graphics: 37th Computer Graphics International Conference, CGI 2020, Geneva, Switzerland, 20–23 October 2020. [[CrossRef](#)]
21. Gosselin, C.; Angeles, J. The Optimum Kinematic Design of a Planar Three-Degree-of-Freedom Parallel Manipulator. *J. Mech. Transm. Autom.* **1988**, *110*, 35–41. [[CrossRef](#)]
22. Cheng, L.; Guohua, C.; Yongyin, Q. Safety Analysis via Forward Kinematics of Delta Parallel Robot using Machine Learning. *Saf. Sci.* **2019**, *117*, 243–249.
23. Swaraj, Z.; Sharad, K.P. Matlab Toolbox for Kinematic Analysis and Simulation of Dexterous Robotic Grippers. In Proceedings of the 12th Global Congress on Manufacturing and Management, GCMM 2014, Procedia Engineering, Vellore, India, 8–10 December 2014; Volume 97, pp. 1886–1895.
24. Carmelo, M.; Stephen, G.P.; Pascual, I.N.; Ian, C. Robotic path Planning for Non-Destructive Testing—A Custom MATLAB Toolbox, Approach. *Robot. Comput.-Integr. Manuf.* **2016**, *37*, 1–12.
25. Ma, L.; Dexue, B.; Zhipeng, X. Mechanism Simulation and Experiment of 3-DOF Parallel Robot Based on MATLAB. In Proceedings of the 2015 International Power, Electronics and Materials Engineering Conference, Dalian, China, 16–17 May 2015.
26. Shehata, M.; Elshami, M.; Bai, Q.; Zhao, X. Parameter Estimation for Multibody System Dynamic Model of Delta Robot from Experimental Data. *IFAC-PapersOnLine* **2021**, *54*, 72–77. [[CrossRef](#)]
27. Cretescu, N.; Neagoe, M.; Saulescu, R. Kinematic and Dynamic Analysis of a 4DOF Parallel Robot with Flexible Links. In Proceedings of the Joint International Conference of the XII International Conference on Mechanisms and Mechanical Transmissions (MTM) and the XXIII International Conference on Robotics (Robotics ’16), Aachen, Germany, 26–27 October 2016; pp. 473–481.
28. Cretescu, N.R.; Neagoe, M. Rigid versus Flexible Link Dynamic Analysis of a 3DOF Delta Type Parallel Manipulator. *Appl. Mech. Mater.* **2015**, *762*, 101–106. [[CrossRef](#)]
29. Rat, N.R.; Neagoe, M. Rigid vs. flexible links dynamic analysis of a 3DOF parallel robot. In Proceedings of the 3rd IEEE International Conference on ASME 2009, DEST ’09, San Diego, CA, USA, 30 August–2 September 2009; pp. 534–539.

30. Kuo, Y.-L. Mathematical modeling and analysis of the Delta robot with flexible links. *Comput. Math. Appl.* **2016**, *71*, 1973–1989. [[CrossRef](#)]
31. Wu, M.; Mei, J.; Zhao, Y.; Niu, W. Vibration reduction of delta robot based on trajectory planning. *Mech. Mach. Theory* **2020**, *153*, 104004. [[CrossRef](#)]
32. Kermanian, A.; Kamali, E.A.; Taghvaeipour, A. Dynamic analysis of flexible parallel robots via enhanced co-rotational and rigid finite element formulations. *Mech. Mach. Theory* **2019**, *139*, 144–173. [[CrossRef](#)]
33. Weiss, C.; Morlock, M.M.; Hoffmann, N.P. Friction induced dynamics of ball joints: Instability and post bifurcation behavior. *Eur. J. Mech.-A/Solids* **2014**, *45*, 161–173. [[CrossRef](#)]
34. Li, Y.; Shang, D.; Fan, X.; Liu, Y. Motion Reliability Analysis of the Delta Parallel Robot considering Mechanism Errors. *Math. Probl. Eng.* **2019**, *2019*, 3501921. [[CrossRef](#)]
35. SIPRO. Available online: <https://www.sipro.vr.it/en/delta-robot/delta-robot-SIAX-D3-1600.html> (accessed on 4 November 2022).
36. Engineeringlibrary. Available online: <https://engineeringlibrary.org/reference/coefficient-of-friction> (accessed on 4 November 2022).

Disclaimer/Publisher's Note: The statements, opinions and data contained in all publications are solely those of the individual author(s) and contributor(s) and not of MDPI and/or the editor(s). MDPI and/or the editor(s) disclaim responsibility for any injury to people or property resulting from any ideas, methods, instructions or products referred to in the content.